Environmental Ocean and Plume Modeling for Deep Sea Mining in the Bismarck Sea

Jade Coulin[a,b], P. J. Haley Jr.[b], Sudip Jana[b], Chinmay S. Kulkarni[b], Pierre F. J. Lermusiaux[b], Thomas Peacock[b]

[a]Paris Tech, France, Paris. Emails: jadec@mit.edu, jade.coulin@mines-paristech.fr
[b]Department of Mechanical Engineering, Massachusetts Institute of Technology,
Cambridge, MA 02139. Emails: phaley@mit.edu, sudip@mit.edu, chinmayk@mit.edu, pierrel@mit.edu, tomp@mit.edu

***Abstract*—A pressing environmental question facing the ocean is the potential impact of possible deep-sea mining activities. This work presents our initial results in developing an ocean and plume modeling system for the Bismark Sea where deep sea mining operations will probably take place. We employ the MSEAS modeling system to both simulate the ocean and to downscale initial conditions from a global system (HYCOM) and tidal forcing from the global TPXO-8 Atlas. We found that at least 1.5 km resolution was needed to adequately resolve the multiscale flow fields. In St. Georges channel, the interaction between the tides, background currents, and underlying density fields increased the subtidal flows. Comparing to historical transport estimates, we showed that tidal forcing is needed to maintain the correct subtidal transport through that Channel. Comparisons with past simulations and measured currents all showed good agreement between the MSEAS hindcasts. Quantitative comparisons made between our hindcasts and independent synoptic ARGO profiles showed that the hindcasts beat persistence by 33% to 50%. These comparisons demonstrated that the MSEAS current estimates were useful for assessing plume advection. Our Lagrangian transport and coherence analyses indicate that the specific location and time of the releases can have a big impact on their dispersal. Our results suggest that ocean mining plumes can be best mitigated by managing releases in accord with such ocean modeling and Lagrangian transport forecasts. Real-time integrated mining-modeling-sampling is likely to provide the most effective mitigation strategies.**

I. Introduction

The impact of human activities on the ocean is becoming increasingly global. One of the pressing environmental questions facing the ocean is the potential impact of the proliferation of deep-sea mining activities. To successfully coexist with the ocean and utilize marine resources, civilization needs to monitor and predict the impacts of its activities [1]. In the past decades, the progress made by combining ocean data and models has been significant [2], [3]. Such data-driven models can forecast ocean properties, such as currents or the dispersal of contaminants. With predictive capabilities, one can also estimate the future impacts of human activities, carry out scenario analyses, and monitor and manage ocean regions and ecosystems [1], [4].

It has long been determined that the sea floor possesses vast untapped resources of rare metals but only recently have they become economically viable. As such, preparations are now underway at the Solwara 1 site off Papua New Guinea (Fig. 1), with operations currently scheduled to start in 2017 [5]. The sea currents in this region have been the subject of only a few studies [6], [7], [8], [9] though the environmental consequences could be important. Although the proposed operations seem sound, there is some concern, that the physical oceanographic and flow transport modeling performed to date is insufficient to rigorously assess the impacts of the project. Of particular concern is whether upwelling and currents could carry pollutants up out of the deep sea, or from spills and leakages into marine food chains where they may affect marine species and the humans that eat them. The high fluctuations of the currents in Saint Georges Channel, a strait south of the Solwara 1 site, and the strong effect of tides require high resolution estimates of the region [7]. All of these impacts need to be further quantified and studied.

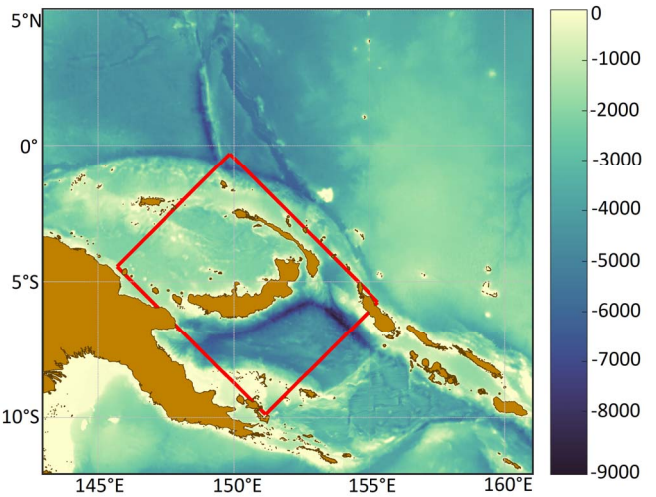

Fig. 1: Modeling domain (red rectangle) and bathymetry employed by the MSEAS hindcast simulations (bathymetry of the region; 143 to 161° horizontally, -12 to 3 ° vertically, scale of the depth: 1,000 m from 0 to 9,000 m).

The long-term goal of our work is to assess the impacts of deep-sea mining by developing a high fidelity, regional, physical-biogeochemical-plume ocean modeling system. Our approach is to build upon the MIT Multidisciplinary Simulation, Estimation and Assimilation System (MSEAS) [10], [11]. MSEAS has been successfully deployed in numerous forecasting and monitoring operations, including forecasting

978-0-692-94690-9/$31.00 ©2017 MTS

the transport of pollutants from the Prestige oil spill [1]. Novel Lagrangian analyses tools can be used to understand three-dimensional flow transports in the region, in order to provide a clearer understanding of the fate of material released by the mining activities at different depths and locations. The tools we implement and develop can be applied to assess the environmental impact at any proposed location for the growing field of deep-sea mining.

In what follows, we present our initial results in developing an ocean and plume modeling system for the Bismark Sea. We outline our system for simulation and forecasting (MSEAS) and describe its set-up for the Bismark Sea (Sect. II). We then compare and contrast hindcasts from different configurations of MSEAS for the Bismark Sea (Sect. III). Next, we assess the skill of the MSEAS hindcasts against independent historical and synoptic data (Sect. IV). Using our MSEAS hindcast flow fields and Lagrangian methods, we then conduct a Lagrangian analysis of the transport of possible plume material (Sect. V). Finally, we present our summary and conclusions (Sect. VI).

II. Modeling system and parameters

A. MSEAS modeling system

MSEAS [10], [11] is used to study and quantify tidal-to-mesoscale processes over regional domains with complex geometries and varied interactions. Modeling capabilities include implicit two-way nesting for multiscale hydrostatic primitive equation (PE) dynamics with a nonlinear free-surface [10] and a high-order finite element code on unstructured grids for non-hydrostatic processes [12], [13]. Additional MSEAS subsystems include: initialization schemes [14], nested data-assimilative tidal prediction and inversion [15]; fast-marching coastal objective analysis [16]; stochastic subgrid-scale models [17], [18]; generalized adaptable biogeochemical modeling system; path planning [19], [20], [21], [22]; Lagrangian Coherent Structures; non-Gaussian data assimilation and adaptive sampling [23], [24], [25], [26], [27]; dynamically-orthogonal equations for uncertainty predictions [28], [29], [30]; and machine learning of model formulations. The MSEAS software is used to provide realistic simulations and predictions in varied regions of the world's ocean [31], [32], [33], [34], [35], [36], for monitoring [1], naval exercises with real-time acoustic-ocean predictions [37], [38] or environmental management [4].

B. MSEAS setup for the Bismarck Sea region

The MSEAS modeling system was set up over a 855.36 km $\times$ 650.43 km region around the Solwara 1 site, in a domain rotated by 45° clockwise for optimal computations (Fig. 1). The model bathymetry was obtained from the 15 arcseconds SRMT15 data ([39]). For this study, many simulations were completed with different horizontal grid resolutions: coarser 3 km and finer 1.5 km resolution with and without tidal forcing. All the modeling setups have 70 vertical levels, with optimized level depths (e.g. higher resolution near the surface). The tidal forcing fields were computed from the high resolution TPSO8-Atlas from OSU and reprocessed for the higher resolution bathymetry and quadratic bottom drag. The bottom drag coefficient value used is 1.6×10^{-3}. Second order Shapiro filter is employed for numerical horizontal filtering, at every time steps, for the tracers, internal velocity, barotropic velocity, and surface pressure. We tested different orders for the Shapiro filter; however, no significant differences were found. The simulations were initialized from the $1/12^\circ$ HYCOM (Hybrid Coordinate Ocean Model) analysis fields of January 15, 2016 [40] and were carried out up to January 31.The velocity fields in the initial condition were optimized for the high resolution coast and bathymetry [14].

We note that in the MSEAS simulations that follow, atmospheric forcing is not utilized. However, in the future, atmospheric fluxes should be used in the boundary condition forcing of the ocean's surface. Similarly, available in situ and remote data could be used for both initialization and assimilation. Higher resolution bathymetry along with implicit 2-way nesting and tiling could further refine the simulation resolution [10]. Ensemble simulations and Dynamically Orthogonal primitive equations can be used for large uncertainty prediction and risk analyses [1], [27], [41], [29], [30].

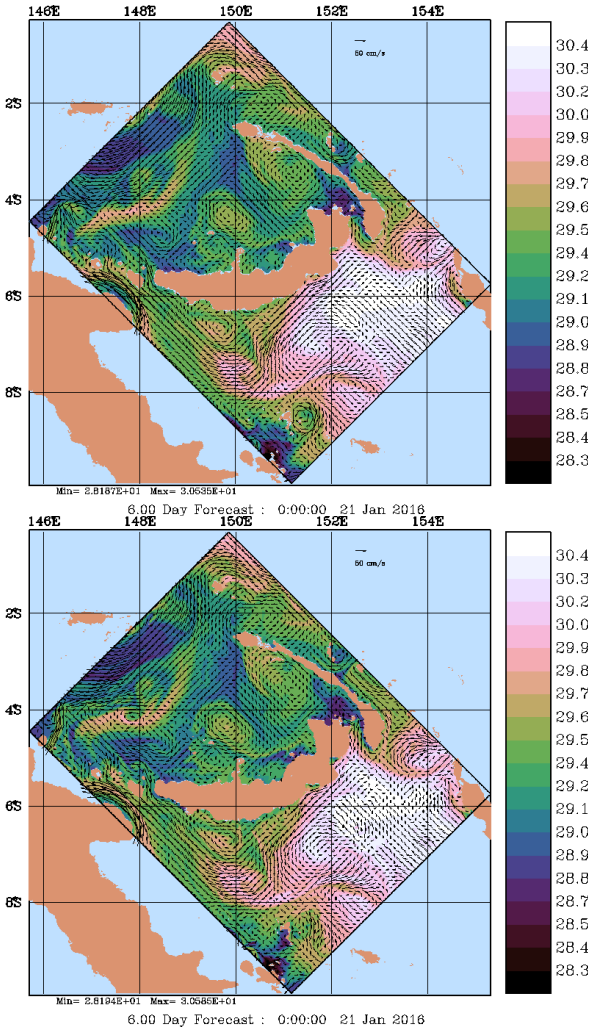

Fig. 2: MSEAS hindcast of surface temperatures on Jan 21, 2016 from 3 km (top) and 1.5 km simulations.

III. MSEAS Ocean Simulation Results for the Bismarck Sea Region

A. *Effect of Modeling Resolution and Tides*

A goal of our study was to show the importance of tides and higher spatial resolution in resolving the multiscale flow fields of this region. Figure 2 compares the surface temperatures and currents on Jan 21, 2016 from the coarser (3 km) and finer (1.5 km) resolution simulations. The finer resolution provides better resolved flow fields and produces more structured eddies and temperature filaments. We notice a variation in the intensity of the currents near the coasts and in some straits with the formation of some small eddies in the 1.5 km simulations.

Figure 3 shows the impacts of spatial resolution and tidal forcing on the simulated currents at 100 m depth in the Saint George's Channel. These impacts are noticeable already 5 days after the Jan 20 initialization. The flow fields at 1.5 km (top left) and 3 km resolution without tides confirm that the finer resolution is needed to resolve channel flows. The finer resolution run produces stronger northward flow around the York island. Furthermore, the finer resolution run with tides results in stronger velocity when compared to its counterpart without tides. Tides modulate the sub-tidal flow through the Strait rather than causing reversals: currents are mostly between 30 and 36 cm/s in the tidal simulation whereas they are between 18 and 24 cm/s in the no-tides simulation. Note that currents at 100 m depth in the runs with and without tides differ especially at the Straits location, where tidal effects are highly noticeable (Fig. 4). This indicates that tides can have a dominant role in the rapid spreading of plumes from the mining site.

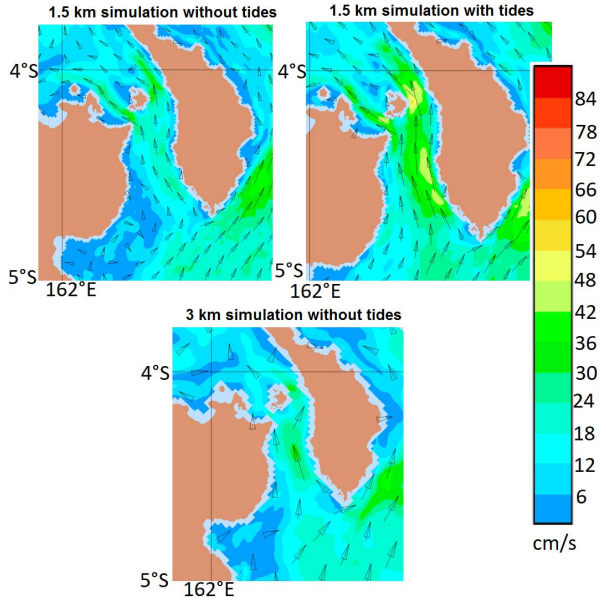

Fig. 3: MSEAS hindcast of currents velocities at 100 m depth in Saint George's Channel on Jan 20, 2016 from 1.5 km simulation without (top left) and with (top right) tides, and 3 km simulation without tides (bottom).

(a) **1.5 km simulation without tide**

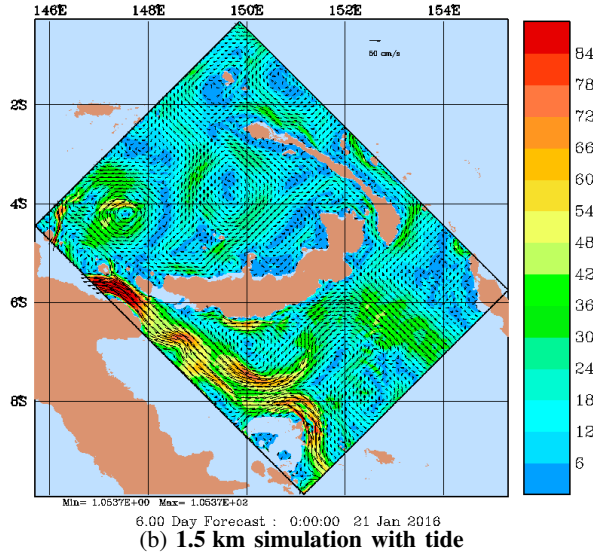

(b) **1.5 km simulation with tide**

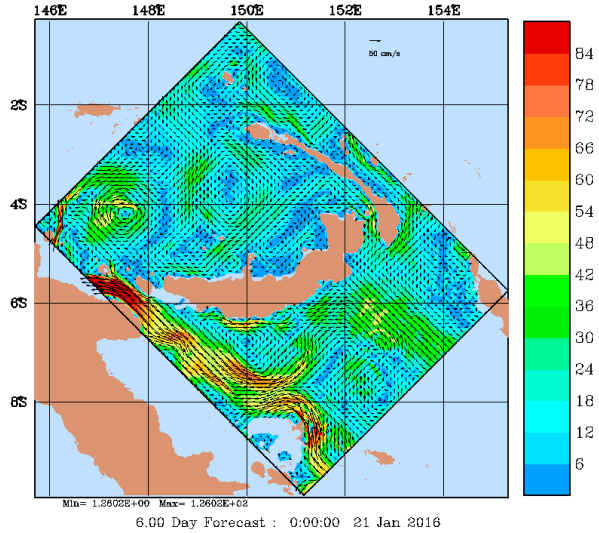

Fig. 4: MSEAS simulated circulation maps at 100 m depth on Jan 21 from 1.5 km simulations with and without tides.

B. *MSEAS Hindcast Simulations for January, 2016*

Figure 5 showcases the time evolution of the multiscale features in the MSEAS simulated surface circulation and temperature fields. The simulated fields from 2 days (Jan 17; left column) and 15 days (Jan 30; right column) after the initialization are compared. As time progresses, the modeling system resolves finer flow features. On Jan 17, the Saint George's Channel experienced a very weak flow and cooler sea surface temperature (SST). However, on Jan 30, a stronger northwestward current flows through the channel, carrying warmer water. This stronger current is due to interactions between the tides, background currents, and underlying density fields. In the region, the background currents are relatively strong and tides only modulate the strength of the density-driven currents rather than cause full reversals.

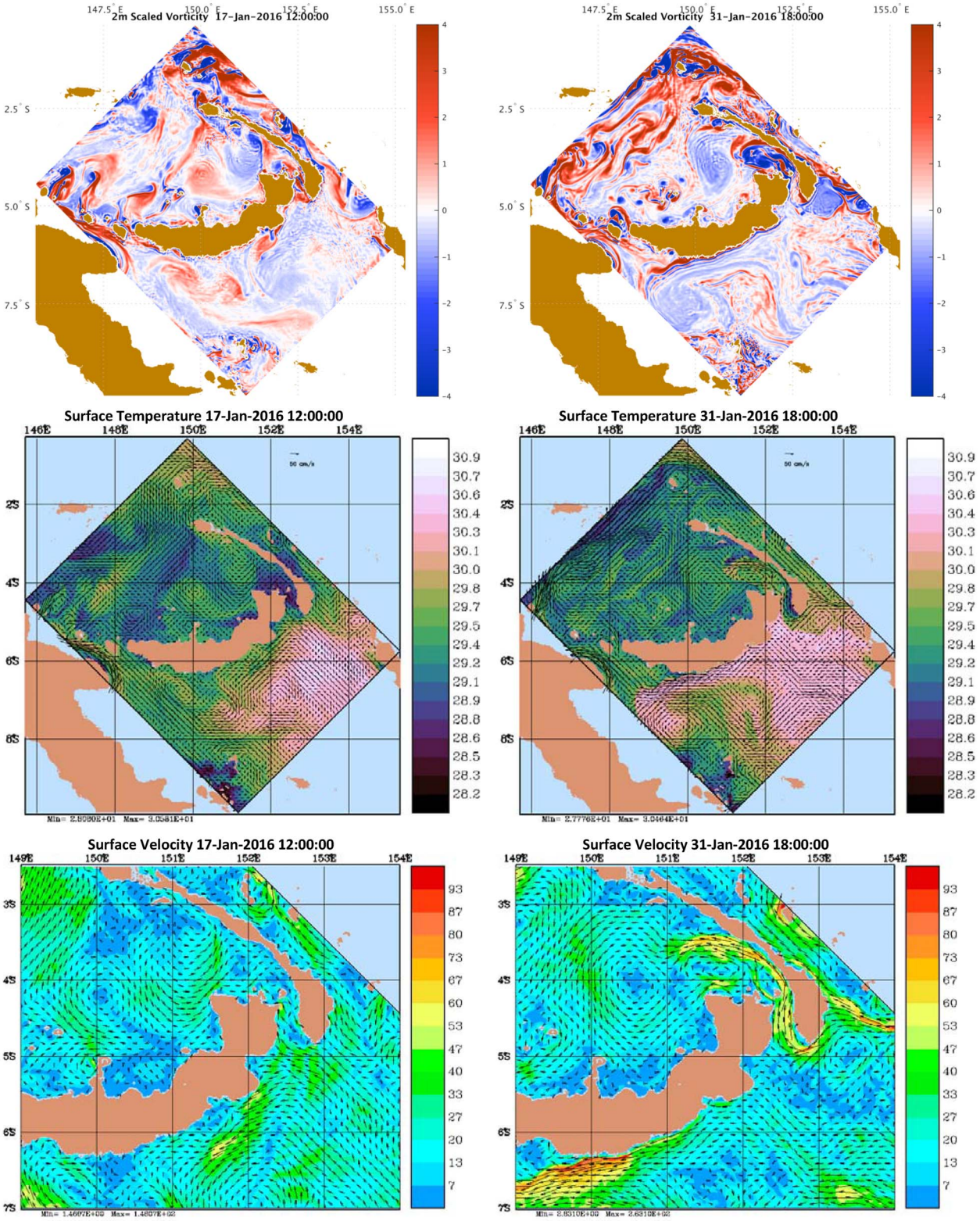

Fig. 5: MSEAS hindcast simulations results: snapshot of 2m-depth scaled vorticity (top row), surface temperature (°C ; middle row) and surface velocity (m/s; zoomed near the mining location; bottom row)) for Jan 17 12:00Z (left column) and Jan 31 18:00Z (right column). The interaction between tides, background current and density fields strengthens the subtidal currents through the straits by Jan 31. The tides modulate the flow through the strait rather than cause reversals.

IV. Evaluation of MSEAS Hindcasts Skill: Comparisons with Prior Results and Independent Synoptic Ocean Data

A. Prior Results

Only a few studies about the Bismarck Sea have been completed, so there is still a lack of detailed knowledge and fine resolution in the circulation and variability estimates, from both observations and simulations results [6], [7], [42], [43], [44], [45], [46], [47], [9], [8]. Several measurements have however been made in the region of the Bismarck Sea. The transports of various currents in the region have been estimated [6] (see Fig. 6 and Fig. 7 for a map of these currents.). Water mass properties and transports in the Solomon Sea have also been estimated [9]. Estimates of the through-channel currents in St. Georges Channel have been constructed from the averages of shipboard ADCP from 6-8 cruises [7].

Current	Section location	Depth and dist. ranges	Volume transport*
EUC	149°E	120-320 m, 1°36'S-2°N	16.6 ± 2.7
NGCU	Vitiaz Strait	40-320 m, 50 km wide	6.1 ± 0.3
NICU	Cape Namarodu	40-320 m, 0-40 km	3.3 ± 0.2
SGU	St Georges Channel	40-300 m, 48 km wide	3.1 ± 0.2

(over the indicated depth and distance range, in Sv)

Fig. 6: Table of the water transports (Sv) by the different currents and their standard deviations, as estimated by [6].

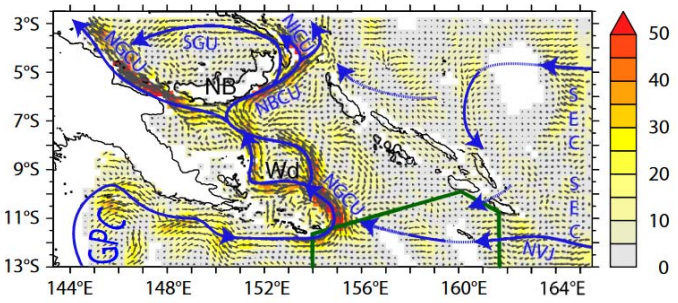

Fig. 7: Map and names of the main currents in the Bismark Sea region, as estimated by [7].

Another set of actual data were the current roses reported by the Solwara mining company about the impacts of their project [5]. They collected data from acoustic Doppler current profiler (ADCP) for over one year at different depths especially at about 1,473 m depth. This depth is close to the bottom depth of the region, because a plan is to release the plume probably 2 m above the sea ground.

The Ocean general circulation model For the Earth Simulator (OFES) hindcast experiment [8] provides a model of near-surface currents (2.5 m depth) collected from mid-December to mid-January every year between 1999 and 2004.

B. Comparison of MSEAS Hindcasts with Prior Results

The first comparison made was between the hindcasts and the estimates of the transports in the region [6]. The yearly quantities of water for the St Georges Undercurrent) (SGU) and the New Ireland Coastal Undercurrent (NICU) are 3.1 +/- 0.2 Sv and 3.3 +/- 0.2 Sv respectively (see Fig. 6). For comparison, we first focus on Fig. 4 where the SGU goes through St. Georges Channel while the NICU goes to east of New Ireland. In our 1.5 km MSEAS hindcast simulation with tides (subplot b), the two currents have almost the same intensity. In the 1.5km MSEAS hindcast simulation without tides (subplot a), the SGU is less intense by one third approximately at 100 m depth. (A comparison of the vertical structure is shown in Fig. 10 and described below). For Vitiaz Strait the effect of the tides is not as important as in St Georges Channel. It is not that surprising because in all the studies tidal effects are described as very large in St Georges Channel but not that important for Vitiaz Strait [6], [7], [46].

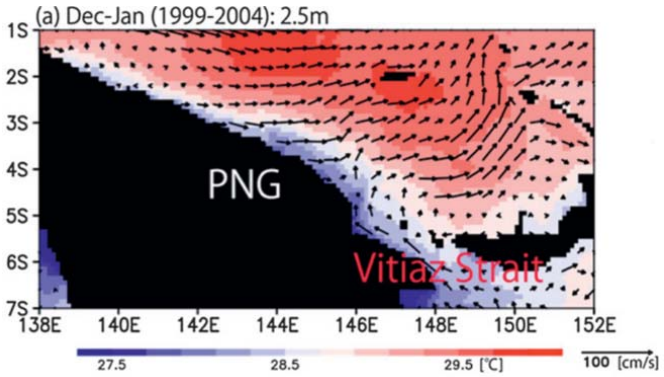

Fig. 8: Map of the mean currents between mid-December and mid-January from 1999 to 2004, as estimated by the OFES hindcast experiment [8].

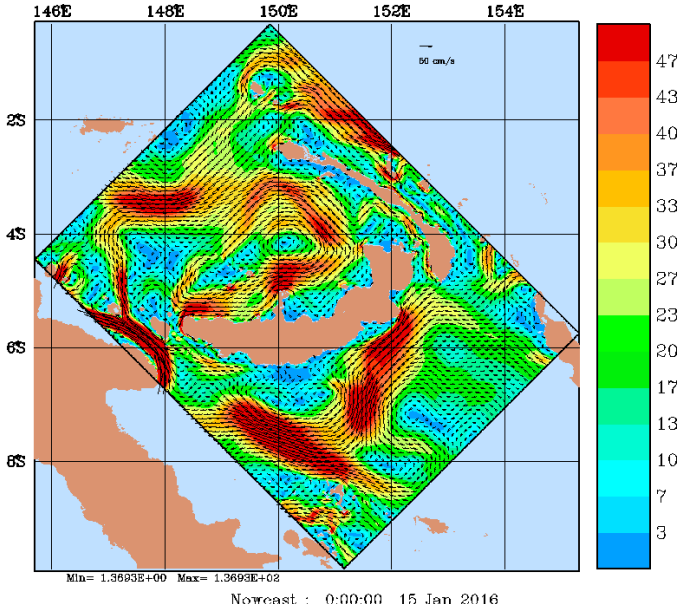

Fig. 9: MSEAS hindcast of velocities on January 15th at 2 m depth for the 1.5 km sumulation (at initialization, downscaled from HYCOM).

OFES Experiment. Another comparison we made was with the OFES results [8] and with the circulation maps of [7]. Fig. 8 shows the means 2.5 m velocities for December-January between 1999-2004. These are compared to the initial conditions (downscaled from HYCOM) for the 1.5 km simulation (Fig. 9) with tides. The currents at the broadest scales are consistent, however many feature in the instantaneous fields are not present in the averaged OFES results. Most notably, the broad cyclonic cirulation in the Bismark Sea is present in the MSEAS simulation but absent in the OFES averaged results. This cyclonic MSEAS feature is however in good agreement with a similar feature in the circulation map of [7] (Fig. 7).

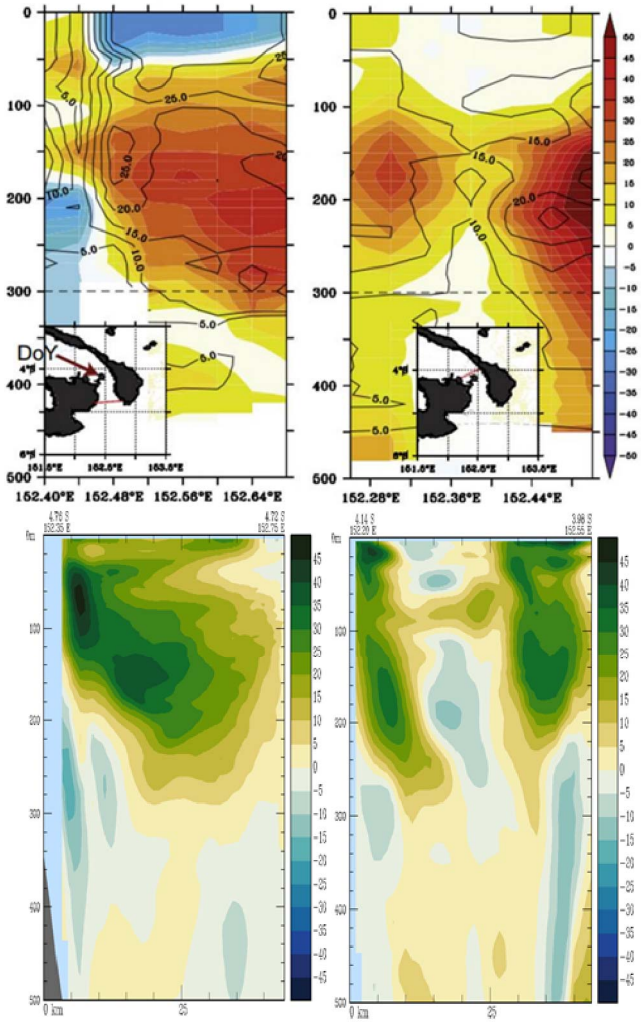

Fig. 10: Comparison of our MSEAS hindcast velocities to historical data. Top row: Average through-channel velocity from ADCP data [7]. Bottom row: Estimates of through-channel currents from hindcast simulations in same sections. The hindcasts currents qualitatively have similar features to the averaged ADCP currents.

Current Roses Data. The ACDP-derived current roses [5] provided another check on our MSEAS hindcast simulations. Despite the lack of resolution of these roses, they can help determining the direction of the currents. With the right month and the right depth ranges, we were able to check if the directions predicted with our model corresponded to these actual data. We only have the simulations for 17 days in January so we could only compared with a few observations, but the comparisons were all satisfactory (not shown).

Average Through-channel Velocity from ADCP Data. We compared estimates of through-channel currents in St. Georges Channel [7] to our MSEAS hindcast simulation estimates of through-channel currents in the same sections, Fig. 10. We see that the MSEAS primitive-equation hindcast currents have features that are qualitatively similar to those of the averaged ADCP data. Some additional tuning is needed to get a better quantitative match. For example, south of St Georges Channel the core of the current in the hindcast is not as deep as it is in the averaged section. We note however that detailed comparisons at different times should not be expected to be perfect: this is because the average of 17 days in January 2016 is in general not the exact same average flow as ADCP current data averaged over another period.

C. Skill of the MSEAS Hindcast Simulations

The comparison of hindcasts to independent in-situ ARGO data allows to evaluate the skill of the MSEAS PE ocean hindcasts simulations as if they were forecasts. This is because a hindcast is a forecast run in the past. To do so, we compare two MSEAS simulation estimates of the ARGO data profile: the one given by the initial condition of the MSEAS hindcast to that of the actual hindcast at the time at which the Argo profile was taken. The former is the so-called persistence forecast, and the latter is the actual forecast: if the latter is closer to the sampled data, one would say that the forecast beats persistence.

In Fig. 11, we show a comparison between the tidally-forced 1.5 km hindcast simulation with the available ARGO data in the modeling domain during the hindcast period (Jan 15-31, 2016). Although no data is assimilated during the hindcast, the forecast skill improves with forecast duration. Specifically on Jan 23, 2016 (top row) the forecast salinity RMSE is 33% smaller than the persistence RMSE. On Jan 29, 2016 (bottom row), the forecast salinity RMSE is 50% smaller than the persistence RMSE. Similar improvements were observed for temperature (not shown). These are significant results. They show the predictive capability of the MSEAS primitive-equation modeling system as set-up for this Bismarck Sea region.

V. Lagrangian Analysis of Plume Transport

The plumes released from the deep sea mining operations are passively advected with the background ocean currents, e.g. [48], and hence their motion and the consequent tracer concentration fields are here predicted by using Lagrangian analysis [49], [50]. To understand the finite-time locally attracting and repelling manifolds in domain, we utilize a novel PDE based flow map computation method [51] that provides high accuracy as well as computational efficiency.

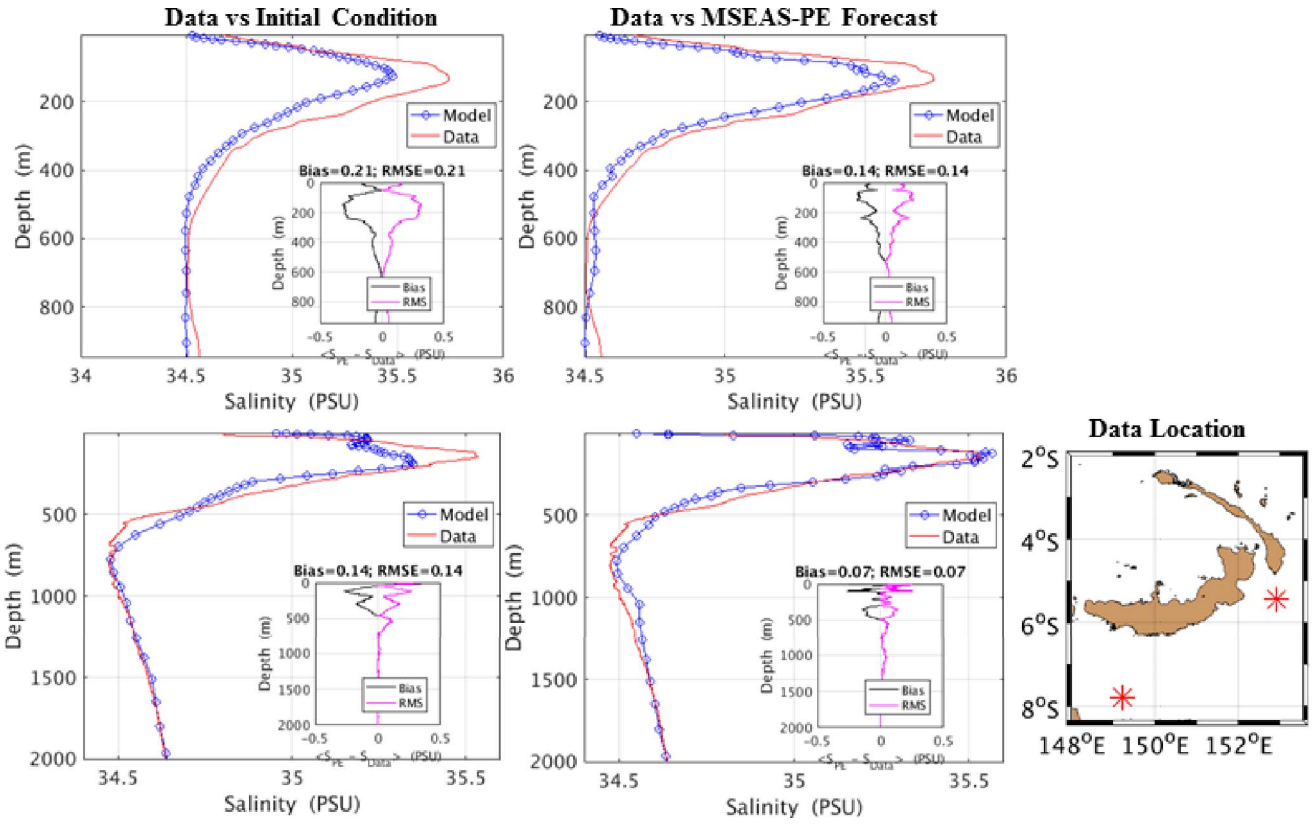

Fig. 11: Comparison of the MSEAS hindcasts to independent in-situ ARGO data. Top row: comparison of persistence and hindcast salinity to Jan 23, 2016 ARGO profile. MSEAS forecast salinity RMSE 33% smaller than persistence. Bottom row: similar comparison for Jan 29, 2016 ARGO profile. MSEAS forecast salinity RMSE 50% smaller than persistence. Similar improvments were observed for temperature.

(a) Backward (attracting) FTLE field

(b) Forward (repelling) FTLE field

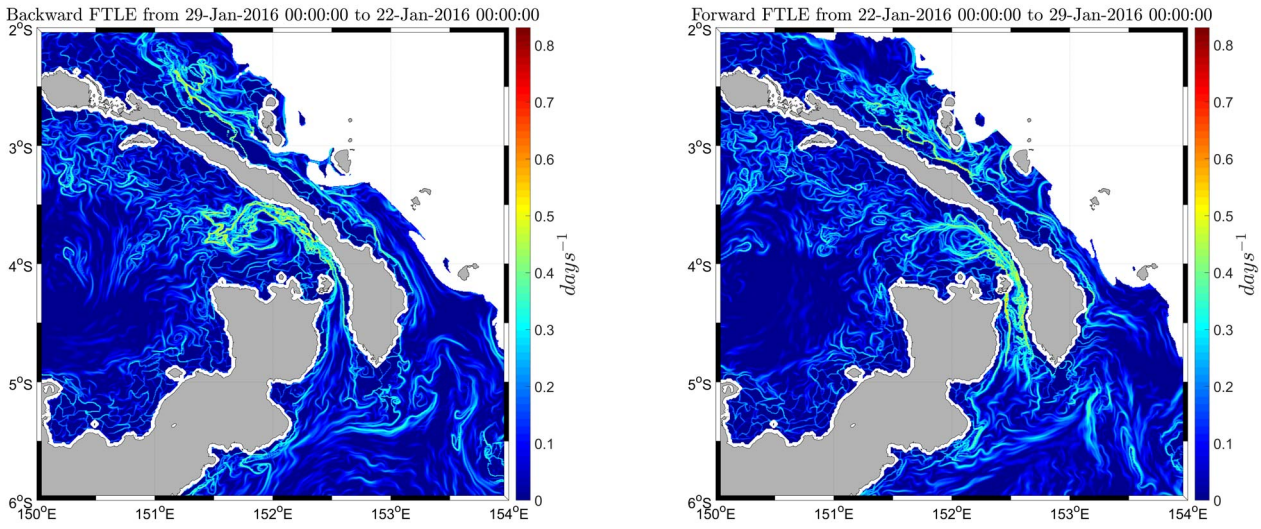

Fig. 12: Backward and forward FTLE fields between January 22, 2016 and January 29, 2016, at a depth of 1275 m. For that period, a repelling manifold is hindcast to be in the St Georges channel, whereas a local attractor is hindcast to be just Northwest of the channel in the Bismark sea.

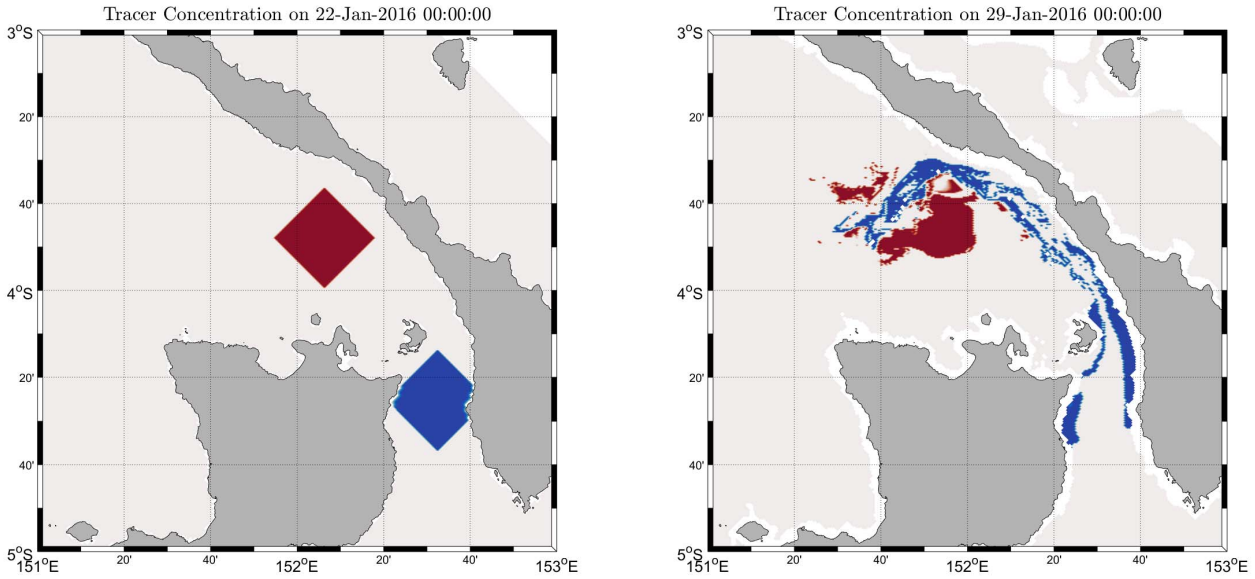

Fig. 13: Transport of the plume material between Jan. 22, 2016 and Jan. 29, 2016. The plume of a simulated material release from the proposed mining site in the Bismark sea is colored in red. Material that could be released from another site that we simulate in the St Georges channel (to illustrate the effect of the attracting and repelling coherent structures) is colored in blue. For that January period in 2016, the material released in the Bismark sea is not transported much, whereas the material released inside the channel is transported out of the channel and into the Bismark sea. Of course, other periods can lead to different results. To minimize environmental impacts, mining releases should likely be managed in accord with ocean forecasts.

Specifically, we study the transport of a plume released at the proposed mining site in the Bismark sea, at a depth of 1275 m. The time domain of interest is over 7 days from January 22, 2016 until January 29, 2016. The attracting and repelling FTLEs (finite time Lyapunov exponents) in the considered region and the considered time period are shown in Figs. 12a and 12b respectively. These FTLE fields suggest that for the Jan. 22-29, 2016 period, there was a locally repelling manifold within the St Georges channel, whereas there was a local attractor just Northwest of the channel.

In order to study the transport of plumes arising from the deep sea mining operations, we look at two possible release sites: one just Northwest of the channel which is the Solwara 1 proposed site [5], and another one inside the channel. Although the latter is not a proposed mining site, it is considered for this study as it illustrates the effect of the attracting and repelling structures in the considered region. Both the plumes are initially assumed to be concentrated in a square box around the considered locations. This material is assumed to have been released on January 22, 2016 00:00:00Z and is advected until January 29, 2016 00:00:00Z. Figure 13 presents the initial and the final concentrations of the plume tracer fields.

It can be seen from Fig. 13 that the material plume released at the proposed mining site in the Bismark sea for that week in January 2016 almost remains in the same region even after 7 days. Whereas, the material released inside St Georges channel flows into the Bismark sea and also gathers at the shallow boundaries of the channel. This is consistent with the description provided by the attracting and repelling FTLE fields in this region, wherein a repelling manifold exists inside the channel and an attracting manifold exists in the Bismark sea, just Northwest of the channel. The material released from the proposed mining site is trapped around the attractor, and hence is minimally transported away from its initial location. The material released inside St Georges channel is repelled by the present repelling manifold. Hence, it either gathers at the sides of the channel or is transported into the Bismark sea, towards the attracting manifold. Thus, a significant fraction of the material released in the channel ends up in the Bismark sea. This simple comparative study indicates that the fate of mining plumes can be highly dependent on the release location. The plumes can be dispersed far away, possibly reaching protected regions, or can remain concentrated in a single region, leading to an accumulation of fine mining particles (which can be good or not, depending on the specifics of the region). These results indicate that adapting and coordinating the time and location of mining releases in accord with ocean and dispersion forecasts such as those presented here could lead to a minimization of undesired environmental impacts.

VI. Conclusion

In this study we presented our initial results in developing an ocean and plume modeling system for the Bismark Sea that is sufficiently resolved for use in monitoring and forecasting the regional transport of material arising from deep-sea mining operations. Using the MSEAS modeling system, we downscaled initial conditions from an operational global model (HYCOM) and tidal forcing from the global TPXO-8

Atlas. We investigated the effect of modeling resolution and tides on the simulations. We found that the higher 1.5 km resolution was needed to adequately resolve the multiscale flow fields. Tidal effects were most noticeable in and around the straits, especially in St. Georges channel (just south of the Solwara 1 mining site). Here the interaction between the tides, background currents, and underlying density fields increased the subtidal flows, leading to stronger currents impinging on the Solwara 1 site.

Qualitative and quantitative comparisons of the MSEAS hincasts were made to available historical and synoptic data. Using transport estimates from [6] we see that tidal forcing is needed to maintain the correct subtidal transport through St Georges Channel. Comparisons with previous simulation studies [8] and current estimates [7] show good agreement between the MSEAS hindcasts and expected currents. Comparisons to historical ADCP data from [7] and [5] show good qualitative agreement. Quantitative comparisons were made between the MSEAS hindcasts and independent synoptic ARGO profiles. The MSEAS forecast skill improved with forecast durations, with the forecast beating persistence by 33% for a 6 day forecast and by 50% for a 14 day forecast. Overall these comparisons show that the simulations provide environmental estimates that can be useful in assessing plume advection.

Our MSEAS Eulerian ocean modeling and Lagrangian transport analyses indicate that ocean mining releases can be best mitigated by managing the plume releases in accord with the ocean modeling and Lagrangian transport forecasts. Lagrangian analyses simulating plume release from the Solwara 1 proposed mining site as well as another site considered within St Georges channel (for illustrative purposes) were conducted. It was observed that the plume material released from the Solwara 1 site was not transported much, whereas material released from the latter site traveled greater distances to end up in the Bismark sea, over a period of 7 days. Ocean data could then be collected now and then to validate and improve the ocean modeling system. Coupled ocean and plume modeling, tracer release simulations, and scenario analyses would then be feasible. Such an integrated mining-modeling-sampling approach is likely to provide the most effective mitigation strategies.

ACKNOWLEDGMENT

The authors would like to thank the members of the MSEAS group for useful discussions. We are grateful to the MIT Environmental Solutions Initiative (MIT-ESI) for Seed Grant research support. We also thank the Office of Naval Research (ONR) and the National Oceanographic Partnership Program (NOPP) for enabling our MSEAS modeling system development and for research support under grant N00014-15-1-2597 (Seamless Multiscale Forecasting) to the Massachusetts Institute of Technology (MIT).

REFERENCES

[1] P. F. J. Lermusiaux, P. J. Haley, Jr, and N. K. Yilmaz, "Environmental prediction, path planning and adaptive sampling: sensing and modeling for efficient ocean monitoring, management and pollution control," *Sea Technology*, vol. 48, no. 9, pp. 35–38, 2007.

[2] A. R. Robinson, P. F. J. Lermusiaux, and N. Q. Sloan III, "Data assimilation," in *The Global Coastal Ocean-Processes and Methods*, ser. The Sea, K. H. Brink and A. R. Robinson, Eds. New York: John Wiley and Sons, 1998, vol. 10, chapter 20, pp. 541–594.

[3] P. F. J. Lermusiaux, P. Malanotte-Rizzoli, D. Stammer, J. Carton, J. Cummings, and A. M. Moore, "Progress and prospects of U.S. data assimilation in ocean research," *Oceanography*, vol. 19, no. 1, pp. 172–183, 2006. [Online]. Available: http://dx.doi.org/10.5670/oceanog.2006.102

[4] G. Cossarini, P. F. J. Lermusiaux, and C. Solidoro, "Lagoon of Venice ecosystem: Seasonal dynamics and environmental guidance with uncertainty analyses and error subspace data assimilation," *Journal of Geophysical Research: Oceans*, vol. 114, no. C6, Jun. 2009, doi:10.1029/2008JC005080.

[5] "Environmental impact statement, solwara 1 project, vol. a. brisbane: Coffey natural systems pty. ltd," 2008. [Online]. Available: http://www.cares.nautilusminerals.com/

[6] J. Butt and E. Lindstrom, "Currents off the east coast of new ireland, papua new guinea, and their relevance to regional undercurrents in the western equatorial pacific ocean," *Journal of Geophysical Research: Oceans*, vol. 99, no. C6, pp. 12 503–12 514, 1994.

[7] S. Cravatte, A. Ganachaud, Q.-P. Duong, W. S. Kessler, G. Eldin, and P. Dutrieux, "Observed circulation in the solomon sea from sadcp data," *Progress in Oceanography*, vol. 88, no. 1, pp. 116–130, 2011.

[8] T. Hasegawa, K. Ando, and H. Sasaki, "Cold water flow and upper-ocean currents in the bismarck sea from december 2001 to january 2002," *Journal of Physical Oceanography*, vol. 41, no. 4, pp. 827–834, 2011.

[9] C. Germineaud, A. Ganachaud, J. Sprintall, S. Cravatte, G. Eldin, M. S. Alberty, and E. Privat, "Pathways and water mass properties of the thermocline and intermediate waters in the solomon sea," *Journal of Physical Oceanography*, vol. 46, no. 10, pp. 3031–3049, 2016.

[10] P. J. Haley, Jr. and P. F. J. Lermusiaux, "Multiscale two-way embedding schemes for free-surface primitive equations in the "Multidisciplinary Simulation, Estimation and Assimilation System"," *Ocean Dynamics*, vol. 60, no. 6, pp. 1497–1537, Dec. 2010.

[11] W. G. Leslie, P. J. Haley, Jr., P. F. J. Lermusiaux, M. P. Ueckermann, O. Logutov, and J. Xu, "MSEAS Manual," Department of Mechanical Engineering, Massachusetts Institute of Technology, Cambridge, MA, MSEAS Report 06, 2010. [Online]. Available: http://mseas.mit.edu/?p=2237

[12] M. P. Ueckermann and P. F. J. Lermusiaux, "High order schemes for 2D unsteady biogeochemical ocean models," *Ocean Dynamics*, vol. 60, no. 6, pp. 1415–1445, Dec. 2010.

[13] ——, "Hybridizable discontinuous Galerkin projection methods for Navier–Stokes and Boussinesq equations," *Journal of Computational Physics*, vol. 306, pp. 390–421, 2016.

[14] P. J. Haley, Jr., A. Agarwal, and P. F. J. Lermusiaux, "Optimizing velocities and transports for complex coastal regions and archipelagos," *Ocean Modeling*, vol. 89, pp. 1–28, 2015.

[15] O. G. Logutov and P. F. J. Lermusiaux, "Inverse barotropic tidal estimation for regional ocean applications," *Ocean Modelling*, vol. 25, no. 1–2, pp. 17–34, 2008. [Online]. Available: http://www.sciencedirect.com/science/article/pii/S1463500308000851

[16] A. Agarwal and P. F. J. Lermusiaux, "Statistical field estimation for complex coastal regions and archipelagos," *Ocean Modelling*, vol. 40, no. 2, pp. 164–189, 2011.

[17] P. F. J. Lermusiaux, "Uncertainty estimation and prediction for interdisciplinary ocean dynamics," *Journal of Computational Physics*, vol. 217, no. 1, pp. 176–199, 2006.

[18] A. Phadnis, "Uncertainty quantification and prediction for non-autonomous linear and nonlinear systems," Master's thesis, Massachusetts Institute of Technology, Department of Mechanical Engineering, Cambridge, Massachusetts, September 2013.

[19] T. Lolla, P. F. J. Lermusiaux, M. P. Ueckermann, and P. J. Haley, Jr., "Time-optimal path planning in dynamic flows using level set equations: Theory and schemes," *Ocean Dynamics*, vol. 64, no. 10, pp. 1373–1397, 2014.

[20] T. Lolla, P. J. Haley, Jr., and P. F. J. Lermusiaux, "Time-optimal path planning in dynamic flows using level set equations: Realistic applications," *Ocean Dynamics*, vol. 64, no. 10, pp. 1399–1417, 2014.

[21] ——, "Path planning in multiscale ocean flows: coordination and dynamic obstacles," *Ocean Modelling*, vol. 94, pp. 46–66, 2015.

[22] D. N. Subramani and P. F. J. Lermusiaux, "Energy-optimal path planning by stochastic dynamically orthogonal level-set optimization," *Ocean Modeling*, vol. 100, pp. 57–77, 2016.

[23] T. Sondergaard and P. F. J. Lermusiaux, "Data assimilation with Gaussian Mixture Models using the Dynamically Orthogonal field equations. Part I: Theory and scheme." *Monthly Weather Review*, vol. 141, no. 6, pp. 1737–1760, 2013.

[24] ——, "Data assimilation with Gaussian Mixture Models using the Dynamically Orthogonal field equations. Part II: Applications." *Monthly Weather Review*, vol. 141, no. 6, pp. 1761–1785, 2013.

[25] T. Lolla and P. F. J. Lermusiaux, "A Gaussian–Mixture Model Smoother for Continuous Nonlinear Stochastic Dynamical Systems: Theory and Schemes," *Monthly Weather Review*, 2017.

[26] ——, "A Gaussian–Mixture Model Smoother for Continuous Nonlinear Stochastic Dynamical Systems: Applications," *Monthly Weather Review*, 2017.

[27] P. F. J. Lermusiaux, "Adaptive modeling, adaptive data assimilation and adaptive sampling," *Physica D: Nonlinear Phenomena*, vol. 230, no. 1, pp. 172–196, 2007.

[28] T. P. Sapsis and P. F. J. Lermusiaux, "Dynamically orthogonal field equations for continuous stochastic dynamical systems," *Physica D: Nonlinear Phenomena*, vol. 238, no. 23–24, pp. 2347–2360, Dec. 2009, doi:10.1016/j.physd.2009.09.017.

[29] ——, "Dynamical criteria for the evolution of the stochastic dimensionality in flows with uncertainty," *Physica D: Nonlinear Phenomena*, vol. 241, no. 1, pp. 60–76, 2012.

[30] M. P. Ueckermann, P. F. J. Lermusiaux, and T. P. Sapsis, "Numerical schemes for dynamically orthogonal equations of stochastic fluid and ocean flows," *Journal of Computational Physics*, vol. 233, pp. 272–294, Jan. 2013.

[31] W. G. Leslie, A. R. Robinson, P. J. Haley, Jr, O. Logutov, P. A. Moreno, P. F. J. Lermusiaux, and E. Coelho, "Verification and training of real-time forecasting of multi-scale ocean dynamics for maritime rapid environmental assessment," *Journal of Marine Systems*, vol. 69, no. 1, pp. 3–16, 2008.

[32] R. Onken, A. Álvarez, V. Fernández, G. Vizoso, G. Basterretxea, J. Tintoré, P. Haley, Jr., and E. Nacini, "A forecast experiment in the Balearic Sea." *Journal of Marine Systems*, vol. 71, no. 1-2, pp. 79–98, 2008.

[33] P. J. Haley, Jr., P. F. J. Lermusiaux, A. R. Robinson, W. G. Leslie, O. Logoutov, G. Cossarini, X. S. Liang, P. Moreno, S. R. Ramp, J. D. Doyle, J. Bellingham, F. Chavez, and S. Johnston, "Forecasting and reanalysis in the Monterey Bay/California Current region for the Autonomous Ocean Sampling Network-II experiment," *Deep Sea Research Part II: Topical Studies in Oceanography*, vol. 56, no. 3–5, pp. 127–148, Feb. 2009, doi:10.1016/j.dsr2.2008.08.010.

[34] A. Gangopadhyay, P. F. Lermusiaux, L. Rosenfeld, A. R. Robinson, L. Calado, H. S. Kim, W. G. Leslie, and P. J. Haley, Jr., "The California Current system: A multiscale overview and the development of a feature-oriented regional modeling system (FORMS)," *Dynamics of Atmospheres and Oceans*, vol. 52, no. 1–2, pp. 131–169, Sep. 2011, Special issue of Dynamics of Atmospheres and Oceans in honor of Prof. A. R. Robinson.

[35] S. R. Ramp, P. F. J. Lermusiaux, I. Shulman, Y. Chao, R. E. Wolf, and F. L. Bahr, "Oceanographic and atmospheric conditions on the continental shelf north of the Monterey Bay during August 2006," *Dynamics of Atmospheres and Oceans*, vol. 52, no. 1–2, pp. 192–223, Sep. 2011, Special issue of Dynamics of Atmospheres and Oceans in honor of Prof. A. R. Robinson.

[36] M. E. G. D. Colin, T. F. Duda, L. A. te Raa, T. van Zon, P. J. Haley, Jr., P. F. J. Lermusiaux, W. G. Leslie, C. Mirabito, F. P. A. Lam, A. E. Newhall, Y.-T. Lin, and J. F. Lynch, "Time-evolving acoustic propagation modeling in a complex ocean environment," in *OCEANS - Bergen, 2013 MTS/IEEE*, 2013, pp. 1–9.

[37] J. Xu, P. F. J. Lermusiaux, P. J. Haley Jr., W. G. Leslie, and O. G. Logutov, "Spatial and Temporal Variations in Acoustic propagation during the PLUSNet-07 Exercise in Dabob Bay," in *Proceedings of Meetings on Acoustics (POMA)*, vol. 4. Acoustical Society of America 155th Meeting, 2008, p. 11.

[38] P. F. J. Lermusiaux, J. Xu, C.-F. Chen, S. Jan, L. Chiu, and Y.-J. Yang, "Coupled ocean–acoustic prediction of transmission loss in a continental shelfbreak region: Predictive skill, uncertainty quantification, and dynamical sensitivities," *IEEE Journal of Oceanic Engineering*, vol. 35, no. 4, pp. 895–916, Oct. 2010.

[39] W. H. Smith and D. T. Sandwell, "Global sea floor topography from satellite altimetry and ship depth soundings," *Science*, vol. 277, no. 5334, pp. 1956–1962, 1997.

[40] J. A. Cummings and O. M. Smedstad, "Variational data assimilation for the global ocean," in *Data Assimilation for Atmospheric, Oceanic and Hydrologic Applications (Vol. II)*. Springer, 2013, pp. 303–343.

[41] P. F. J. Lermusiaux, P. J. Haley, W. G. Leslie, A. Agarwal, O. Logutov, and L. J. Burton, "Multiscale physical and biological dynamics in the Philippine Archipelago: Predictions and processes," *Oceanography*, vol. 24, no. 1, pp. 70–89, 2011, Special Issue on the Philippine Straits Dynamics Experiment.

[42] S. Cravatte, W. S. Kessler, and F. Marin, "Intermediate zonal jets in the tropical pacific ocean observed by argo floats," *Journal of Physical Oceanography*, vol. 42, no. 9, pp. 1475–1485, 2012.

[43] F. Gasparin, A. Ganachaud, C. Maes, F. Marin, and G. Eldin, "Oceanic transports through the solomon sea: the bend of the new guinea coastal undercurrent," *Geophysical Research Letters*, vol. 39, no. 15, 2012.

[44] A. Melet, L. Gourdeau, J. Verron, and B. Djath, "Solomon sea circulation and water mass modifications: response at enso timescales," *Ocean Dynamics*, vol. 63, no. 1, pp. 1–19, 2013.

[45] B. Djath, A. Melet, J. Verron, J.-M. Molines, B. Barnier, L. Gourdeau, and L. Debreu, "A 1/36 model of the solomon sea embedded into a global ocean model: On the setting up of an interactive open boundary nested model system," *Journal of Operational Oceanography*, vol. 7, no. 1, pp. 34–46, 2014.

[46] B. Djath, J. Verron, A. Melet, L. Gourdeau, B. Barnier, and J.-M. Molines, "Multiscale dynamical analysis of a high-resolution numerical model simulation of the solomon sea circulation," *Journal of Geophysical Research: Oceans*, vol. 119, no. 9, pp. 6286–6304, 2014.

[47] A. Ganachaud, S. Cravatte, A. Melet, A. Schiller, N. Holbrook, B. Sloyan, M. Widlansky, M. Bowen, J. Verron, P. Wiles *et al.*, "The southwest pacific ocean circulation and climate experiment (spice)," *Journal of Geophysical Research: Oceans*, vol. 119, no. 11, pp. 7660–7686, 2014.

[48] R. Camilli, C. M. Reddy, D. R. Yoerger, B. A. Van Mooy, M. V. Jakuba, J. C. Kinsey, C. P. McIntyre, S. P. Sylva, and J. V. Maloney, "Tracking hydrocarbon plume transport and biodegradation at deepwater horizon," *Science*, vol. 330, no. 6001, pp. 201–204, 2010.

[49] G. Haller, "Lagrangian coherent structures," *Annual Review of Fluid Mechanics*, vol. 47, pp. 137–162, 2015.

[50] T. Peacock and G. Haller, "Lagrangian coherent structures: The hidden skeleton of fluid flows," *Physics today*, vol. 66, no. 2, pp. 41–47, 2013.

[51] C. S. Kulkarni and P. F. J. Lermusiaux, "Method of composition for the computation of finite time lyapunov exponent in dynamic flow fields," in preparation.